Journal of Experimental and Theoretical Physics, Vol. 101, No. 4, 2005, pp. 646–652.
Translated from Zhurnal Éksperimental'noĭ i Teoreticheskoĭ Fiziki, Vol. 128, No. 4, 2005, pp. 752–759.

NUCLEI, PARTICLES, FIELDS, GRAVITATION, AND ASTROPHYSICS

Analysis of Small-Scale Wave Structures in the Saturnian A Ring Based on Data from the Cassini Interplanetary Spacecraft

E. B. Postnikov[a] and A. Yu. Loskutov[b]

[a] *Kursk State University, ul. Radishcheva 33, Kursk, 305000 Russia*
[b] *Moscow State University, Vorob'evy gory, Moscow, 119992 Russia*
e-mail: loskutov@chaos.phys.msu.ru

Received April 19, 2005

Abstract—The images obtained during the second half of 2004 by the Cassini interplanetary spacecraft are analyzed. The method of analysis is based on the original algorithm of a continuous wavelet transform with a complex Morlet wavelet that reduces the integral transform to solving a Cauchy problem for a system of partial differential equations. This method is shown to be a fairly efficient tool for analyzing the instant variable periodicity of the spatial particle inhomogeneity in the radial structure of Saturn's rings. © *2005 Pleiades Publishing, Inc.*

1. INTRODUCTION

The structure of planetary rings generally and Saturn's rings specifically arouses constant scientific interest in studying them as a dynamical system of many particles (see, e.g., [1] for an overview of the status of the problem as of 2002 and references). A characteristic feature of Saturn's main rings (A, B, C) is their small-scale structure detected by the Voyagers. Its preliminary analysis (see [2–4]) led to a model for the formation of thin spiral density waves through the resonant interaction of ring particles with Saturnian satellites.

Subsequently, a window Fourier transform was used to analyze the Voyager data on the A ring [5]. This analysis revealed and identified about 40 resonance structures attributed to the influence of various Saturnian satellites. At the same time, the authors of [5] pointed out a number of resonance regions in which the achieved resolution and the capabilities of the processing algorithm did not allow any features in the ring matter distribution to be detected.

Over the last year, the data obtained by the Cassini spacecraft, including high-resolution photographs (see [6] for a preliminary report of the Cassini task group), have opened up new opportunities for studies in this field. The wavelet transform, a method of analysis that has been actively developed in the past two decades, can be used to process them. An important advantage of this technique over other approaches (see, e.g., [7]) is a high degree of localization of the basis function in both the spatial and frequency domains. This allows nonstationary signals to be effectively studied based on the concept of an instant frequency (or period). The interrelationship between the window width and the instant period (the window contracts for high-frequency signals and expands for low-frequency signals; as a result, the effective number of oscillations of the basis sine wave in the window is conserved) favorably distinguishes the wavelet transform from the window Fourier transform.

As applied to celestial mechanics, the wavelet analysis method has shown its efficiency in processing the solution functions generated by Hamiltonian systems, in particular, in the three-body problem [8] and in studying the variations in the revolution periods of asteroids in near-resonance regions [9]. As applied to the Saturnian system, the wavelet transform was suggested to be used to study the structure of the Encke gap based on Voyager-2 data [10]. Since the main objective of the authors of the cited paper was to identify structures of various scales in a noisy image, only real wavelets were used. However, determining the pattern of local periodicity in Saturn's ring structure requires using a transform with a complex wavelet. The possible efficiency of such an approach to this problem was demonstrated with specific examples in [6, 11].

The main goal of this paper is to study the small-scale structure of Saturn's A ring using a new approach to calculating the complex integral transform with a Morlet wavelet based on the representation of the wavelet transform as the solution to a system of partial differential equations.

2. DESCRIPTION OF THE METHOD

The most suitable method for solving the problem of distinguishing the instant period in a signal is the com-

plex continuous wavelet transform

$$w(a, b) = \int_{-\infty}^{\infty} f(t)\psi^*\left(\frac{t-b}{a}\right)\frac{dt}{a} \quad (1)$$

(the asterisk denotes complex conjugate) in the amplitude normalization

$$\int_{-\infty}^{\infty}\left|\psi\left(\frac{t-b}{a}\right)\right|\frac{dt}{a} = \text{const} \quad (2)$$

with the Morlet basis. In the exact form that satisfies the admissibility condition

$$\int_{-\infty}^{\infty}\psi(\xi)d\xi = 0,$$

it is

$$\psi(\xi) = \frac{1}{\sqrt{2\pi}} \times\left[\exp(-i\omega_0\xi) - \exp\left(-\frac{\omega_0^2}{2}\right)\right]\exp\left(-\frac{\xi^2}{2}\right). \quad (3)$$

The corresponding wavelet transform $w(a, b)$ acts as a local spectral distribution in periods a of the harmonics that constitute the signal in the neighborhood of point b.

However, in most practical applications, the second term in Eq. (3) is disregarded if the basis frequency is fairly high (in general, $\omega_0 \geq 5$), and the following simplified definition is used:

$$\psi(\xi) = \frac{1}{\sqrt{2\pi}}\exp(-i\omega_0\xi)\exp\left(-\frac{\xi^2}{2}\right). \quad (4)$$

It corresponds to normalization (2) with const = $\exp(\omega_0^2/2)$. A significant advantage of this approximation is the simple relationship between the instant period of the wavelet transform and the period of the harmonic oscillation with frequency ω. In other words, the two-dimensional plot of the distribution of the modulus of the wavelet transform for a complex monochromatic function has a line of maximum that corresponds to the period $a = \pm\omega_0/\omega$. The factor, which is a Gaussian function, performs a smoothing that automatically suppresses the signal noise. The relationship also remains valid for a real function.

Varying the basis frequency allows the frequency resolution to be changed: the higher the frequency ω_0, the more oscillations the basis wavelet function executes on the characteristic window width and the closer the modulus of the wavelet transform to the locally smoothed Fourier spectrum. At low ω_0, it reveals an individual spike.

It should be noted that, despite such advantages as the simplicity of the algorithm and the high speed of calculations, the standard method for calculating the continuous wavelet transform associated with the intermediate passage to the frequency domain and with the use of the fast Fourier transform algorithm has a number of shortcomings. The latter follow from peculiarities of the fast Fourier transform: the initial data must be represented by a sample of 2^N equidistant nodes. Departures from this condition lead to a significant complication of the calculations and/or loss of accuracy.

Therefore, in this paper, we introduce an alternative algorithm based on the observation that the transform obtained by the convolution with the Morlet wavelet satisfies the differential equation

$$\left(a\frac{\partial^2}{\partial b^2} - \frac{\partial}{\partial a} - i\omega_0\frac{\partial}{\partial b}\right)w(a, b) = 0. \quad (5)$$

The latter was derived in [12], but it was used only to demonstrate the local properties of the a priori known wavelet transform.

Let us represent the result of the wavelet transform as a sum of the real and imaginary parts:

$$w(a, b) = u(a, b) + iv(a, b),$$

for which Eq. (5) can be written as the system

$$\frac{\partial u}{\partial a} = a\frac{\partial^2 u}{\partial b^2} + \omega_0\frac{\partial v}{\partial b}, \quad (6)$$

$$\frac{\partial v}{\partial a} = a\frac{\partial^2 v}{\partial b^2} - \omega_0\frac{\partial u}{\partial b}. \quad (7)$$

To find the corresponding initial conditions, let us write the integral transform (1) with kernel (4) as

$$w(a, b) = \int_{-\infty}^{\infty} f(t)\frac{\exp\left[-\frac{1}{2}\left(\frac{t-b}{a} - i\omega_0\right)^2\right]}{\sqrt{2\pi a^2}}dt.$$

This integral is known to be independent of the imaginary subtrahend in the exponent, and the kernel of the transform in the limit $a \longrightarrow 0$ is a delta function. Consequently, $w(0, b) = f(b)$. The initial conditions for the system of differential equations (6) and (7) follow from the latter equality:

$$u(0, b) = \text{Re}(f(b)),$$

$$v(0, b) = \text{Im}(f(b)).$$

The modulus of the wavelet transform required for our

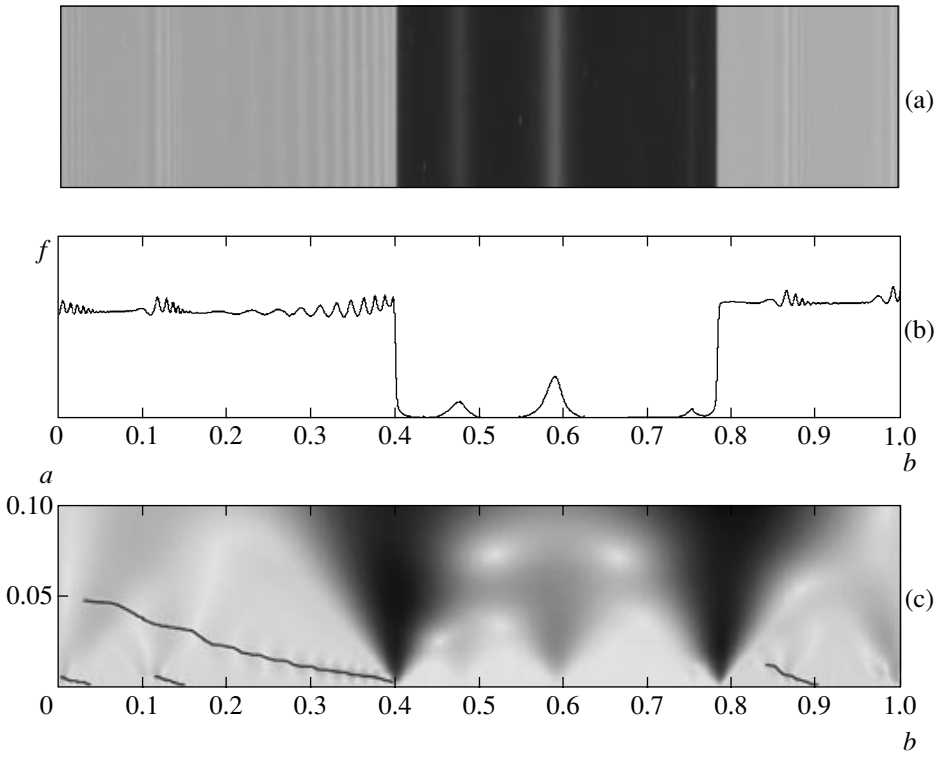

Fig. 1. The Encke gap. The coordinate origin almost coincides with the position of the 11 : 10 resonance with Pandora. The next wave structure is generated by the 15 : 14 resonance with Prometheus. The first wave train after the gap is generated by the 12 : 11 resonance with Pandora.

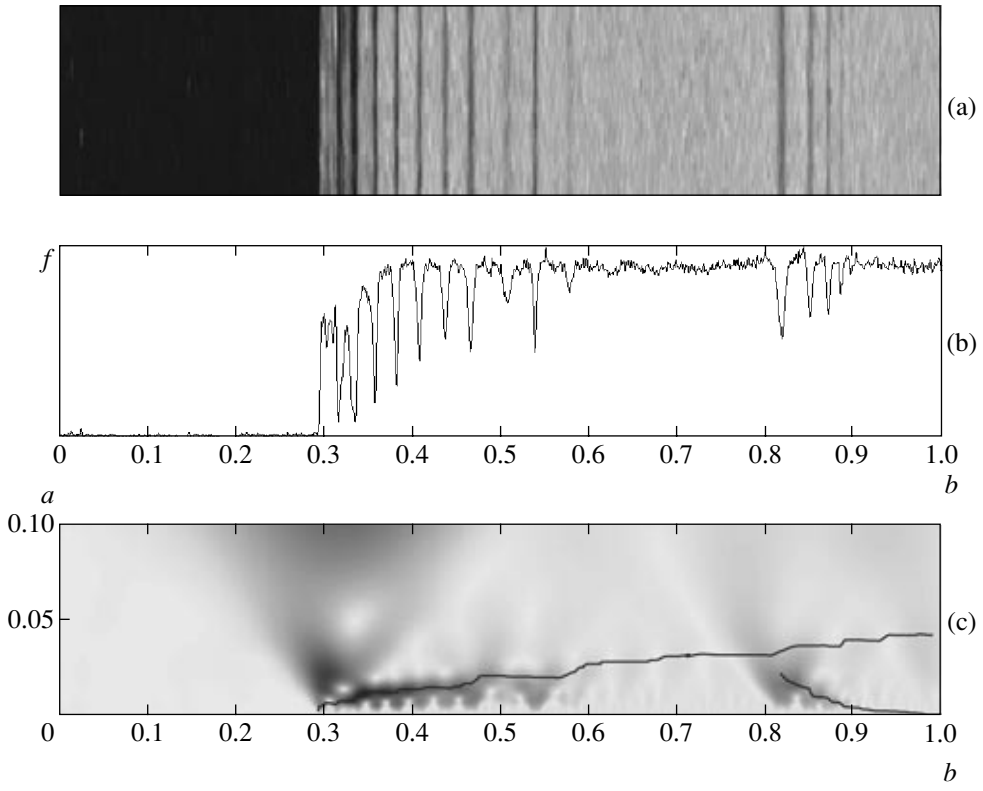

Fig. 2. The far (from Saturn) edge of the Encke gap.

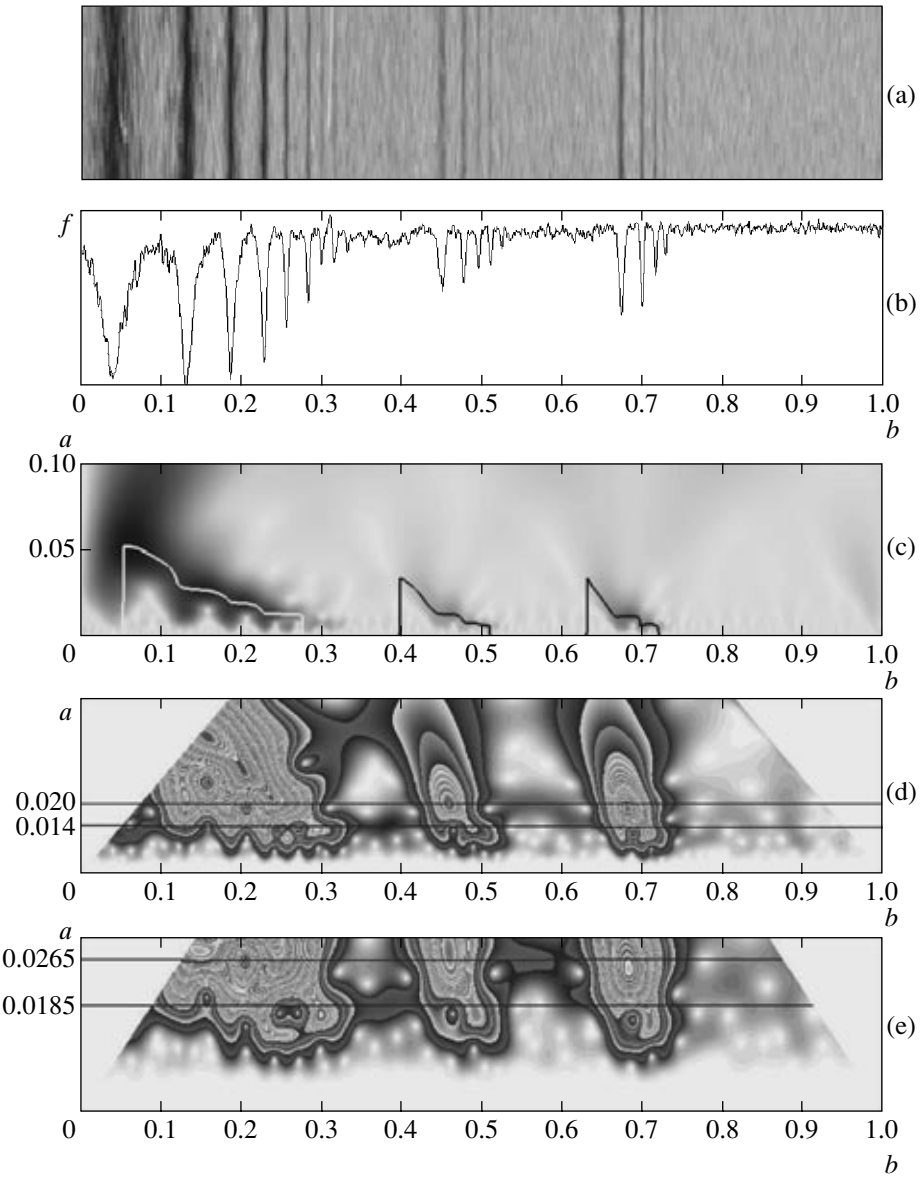

Fig. 3. The outer part of the A ring containing the 4 : 3, 6 : 5, and 7 : 6 resonance with Janus, Pandora, and Prometheus, respectively.

analysis can be easily calculated:

$$|w(a, b)| = \sqrt{u^2(a, b) + v^2(a, b)}.$$

3. IMAGE PROCESSING RESULTS FOR SEGMENTS OF THE A RING

We use the algorithm described above to analyze the radial matter density distribution at the center of Saturn's A ring based on photographic data from the Cassini spacecraft (July 2004). For our analysis, we chose images from the NASA/JPL/Space Science Institute collection. A narrow stripe was separated from each image in the radial direction: PIA06099 (1022 × 20 pixels, Fig. 1a), PIA06094 (891 × 23 pixels, Fig. 2a), PIA06095 (902 × 23 pixels, Fig. 3a), and PIA06093 (855 × 20 pixels, Fig. 4a). It is easy to verify that the curvature of the structures constituting the ring within each sample may be disregarded. For clarity, all images were significantly stretched in the transverse direction.

We used the pair of initial conditions $u(0, b) = f(b)$ and $v(0, b) = 0$, where the function $f(b)$ is obtained by averaging over the sample (Figs. 1b–4b). Since the signal length is finite, the Cauchy problem for Eqs. (6) and (7) must be replaced with a boundary-value problem. We used boundary conditions of the first kind: respectively, the initial signal value at these points and zero for the real and imaginary parts of the wavelet transform.

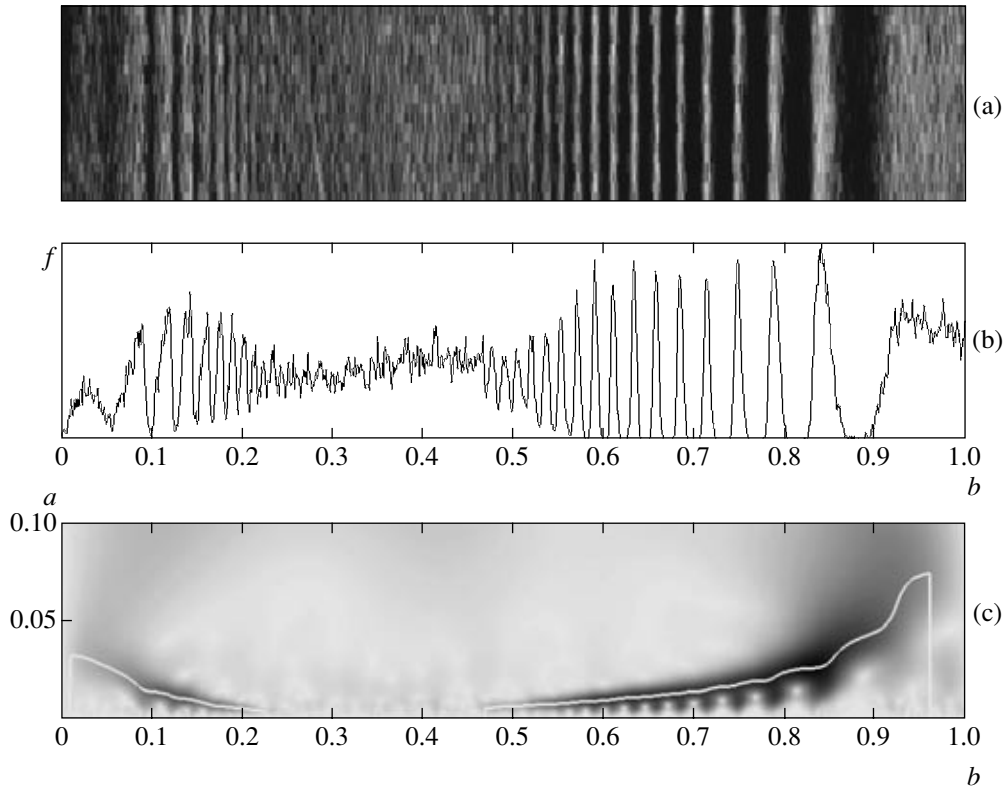

Fig. 4. The density waves generated by the 12 : 11 and 5 : 3 resonances with Prometheus and Mimas, respectively.

Values that are sufficiently high and convenient for interpreting the results should be chosen for the basis frequency. The frequencies $\omega_0 = \pi$ (Figs. 1c–4c), 1.5π (Figs. 3d and 5b), and 2π (Fig. 3c and 5c) in dimensionless units of the sample length satisfy these conditions. At the last two basis frequencies, the regions distorted by the edge effect were removed from the figures. A quantitative criterion for this in the (b, a) plane is the condition

$$\exp\left(-\frac{(b-b_0)^2}{2a^2}\right) \geq 10^{-5},$$

where $b_0 = 0$ or 1.

The image being processed (Fig. 1a) represents the neighborhood of the Encke gap. A characteristic feature that is not revealed by the window Fourier transform is the possibility of tracing the distribution of the instant spatial period of the wave structure of the Encke gap edge. In the plot of the modulus of the wavelet transform (Fig. 1c), the lines of maxima are painted black. Note that the large-scale development of a spiral density wave, which is accompanied by an increase in its instant period, admits of a continuous passage to the line of maximum corresponding to the large-scale spikes. As follows from Fig. 1c, the characteristic size on such scales is on the order of the extent of the train of resonant waves generated by the 11 : 10 and 15 : 14 resonances with the satellites Pandora and Prometheus, respectively. There is a clear overlap between the lines of maxima of various resonances (Fig. 1c). A similar structure (but without a detailed analysis) has also been revealed recently [6]. However, only one line of maximum may be preserved in our approach, which allows relatively low ω_0 to be used. We also found a similar overlap between the lines of maximum of the instant period for the small-scale and large-scale (formed by Pan) resonant wave structures in the outer part of the Encke gap (Fig. 2).

Another type of inhomogeneity that the suggested wavelet analysis method can reveal consists in the presence of a small-scale periodicity in the interresonance intervals. The high (up to 270 m per pixel) resolution of the Cassini images and the algorithm described above, which admits (in view of the peculiarities of the numerical solution of differential equations) of a small step in scale variable, makes such a study possible.

To analyze in detail the small-scale structure in the interresonance region, let us consider the density waves generated by the resonances of Janus, Pandora, and Prometheus. The characteristic ladder form of their instant spatial period is shown in Fig. 3c. To achieve a higher spatial resolution, let us increase the basis frequency to $\omega_0 = 1.5\pi$ (Fig. 3d) and 2π (Fig. 3e). To increase the sensitivity to the modulus of a low amplitude, we will use various shades of gray for high values. This leads to a smearing of the resonance lines, allow-

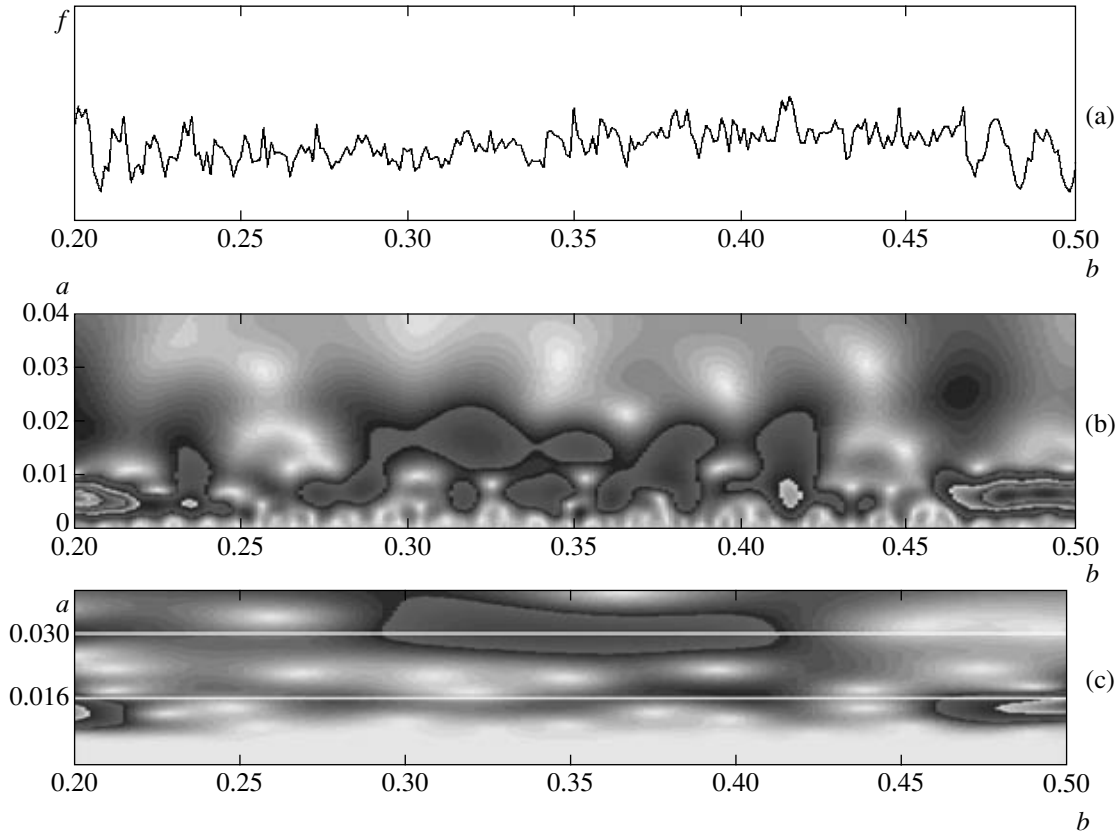

Fig. 5. The region between the 12 : 11 and 5 : 3 resonances with Prometheus and Mimas, respectively.

ing an almost stably periodic signal on the segment [0.35, 0.45] connecting the first two resonant wave trains to be highlighted by brightness lines. A short-wavelength signal is also detected on the segment [0.52, 0.67] between the second and third resonances. However, it has an unstable spatial frequency varying within the range 75π–107π (in units of the sample length). The second frequency is equal to the frequency of the wave between the resonances of Janus (4 : 3) and Pandora (6 : 5). Its refinement using the basis frequency $\omega_0 = 2\pi$ yields $108(\pm1)\pi$ and confirms the stability of the monochromaticity.

The spiral density waves in Fig. 4 generated by the resonances of Prometheus (12 : 11) and Mimas (5 : 3) are among the most distinct in Saturn's ring structure. For this reason, they were studied in detail and modeled using Voyager data (see the earlier papers [2–4] and [5]). Let us analyze the interresonance region by the wavelet method using a recent Cassini photograph. Analysis of the images obtained by a transform with a high frequency resolution (Figs. 5b, 5c) reveals no stable periodicity in this region. However, the existence of an unstable signal with a spatial frequency of 125π (see Fig. 5c, where the lines of maxima are painted white) can be easily seen. In fact, it is close to the highest frequency of the resonant trains. In addition, a short region of more intense periodicity with a frequency of 67π occupying the segment [0.30, 0.41] of the signal under study is revealed. Examining the feature of the instant period on the segment [0.36, 0.38] with a shape similar to the resonance inclined line of the instant period, we can assume that the frequency of 67π is related to the longest-wavelength resonant perturbations.

4. CONCLUSIONS

Thus, the continuous wavelet transform with a complex Morlet wavelet is an efficient tool for studying the spatial radial structure of Saturn's rings. It enables the evolution of the instant period to be traced in detail on various scales. A detailed analysis of the wave processes in Saturn's ring matter should include the interaction of the long-wavelength perturbation segments with the small-scale wave trains generated by the resonant interaction with other satellites and the formation mechanisms of nearly monochromatic waves in the regions connecting the high-frequency ends of the resonant zones.

The main results that allow a wavelet analysis of high-resolution Cassini images to be performed are the following. There are overlaps between the lines of the instant period of the resonant waves generated by Pan and the smaller-scale wave trains generated by other satellites near both boundaries of the Encke gap. In

addition, nearly monochromatic waves of various extents, up to the joining of the resonant trains, can be present in the interresonance regions.

It should be noted that our analysis is preliminary one and is in further elaboration with allowance made for the image adjustment depending on the inclination at which the photographs were taken and the absolute distances to the region of the rings under study.

REFERENCES

1. L. W. Esposito, Rep. Prog. Phys. **65**, 1741 (2002).
2. F. H. Shu, J. N. Cuzzi, and J. J. Lissauer, Icarus **53**, 185 (1983).
3. F. H. Shu, C. Yuan, and J. J. Lissauer, Astrophys. J. **291**, 356 (1985).
4. F. H. Shu, C. Yuan, and J. J. Lissauer, Astrophys. J. **299**, 542 (1985).
5. L. J. Spilker, S. Pilorz, L. A. Lane, *et al.*, Icarus **171**, 373 (2004).
6. C. C. Porco, E. Baker, J. Barbara, *et al.*, Science **307**, 1226 (2005).
7. *The Transforms and Applications Handbook*, Ed. by A. Poularikas (IEEE Press, New York, 2000).
8. L. V. Vela-Arevalo, PhD Thesis (Caltech, 2002).
9. T. A. Michtchenko and D. Nesvorný, Astron. Astrophys. **313**, 674 (1996).
10. Ph. Bendjoya, J.-M. Petit, and F. Spahn, Icarus **105**, 385 (1993).
11. E. B. Postnikov and A. Loskutov, astro-ph/0502375.
12. M. Haase, in *Paradigms of Complexity*, Ed. by M. M. Novak (World Sci., Singapore, 2000), p. 287.

Translated by V. Astakhov